

Regular and irregular dynamics of Dirac-Weyl wavepackets in a mesoscopic quantum dot at the edge of topological insulator

D.V. Khomitsky¹, A.A. Chubanov, A.A. Konakov

Department of Physics, University of Nizhny Novgorod, 603950 Gagarin Avenue 23, Nizhny Novgorod, Russian Federation

Abstract

The dynamics of Dirac-Weyl spin-polarized wavepackets driven by periodic electric field is considered for the electrons in a mesoscopic quantum dot formed at the edge of two-dimensional HgTe/CdTe topological insulator with Dirac-Weyl massless energy spectra, where the motion of carriers is less sensitive to disorder and impurity potentials. It is found that the interplay of strongly coupled spin and charge degrees of freedom creates the regimes of both regular and irregular dynamics with certain universal properties manifested both in the clean limit and in the presence of the moderate disorder. The disorder influence is predicted to enhance the in-plane spin relaxation, leading to possibility of establishing novel types of driven evolution in nanostructures formed in the topological insulators.

Keywords: Dirac-Weyl fermion, topological insulator, magnetic barrier, dynamics, wavepacket, quantum chaos

1. Introduction

Recently a growing attention in various field of fundamental science has been started to focus on the properties of so called Dirac-Weyl fermions [1, 2]. Among their numerous manifestations we can mention here just few examples in quantum field theory [3, 4], conventional and novel condensed matter systems such as ferromagnets[5], graphene [6], or newly emerged topological insulators (TI) [7]. Topological insulators are sometimes called a novel state of matter, representing the condensed matter state where the edge states are protected from backscattering by symmetry existing at the edges of the sample and having energies within the bulk gap. Thus, in TI an efficient transport through edge

Email address: khomitsky@phys.unn.ru (D.V. Khomitsky)

¹Corresponding author

channels can be produced. In the Dirac-Weyl materials the electron dispersion can be described by the massless Hamiltonian of the form

$$H_0 = Ak_i\sigma_j, \tag{1}$$

where the parameter A plays the role of the effective electron velocity, and k_i and σ_j are one of the wavevector components and the Pauli spin matrices, depending on the system geometry. The spectral and dynamical properties of the electrons in Dirac-Weyl materials, mostly in TI, were studied mainly for regular types of the non-stationary evolution induced by external driving fields. These materials included the Floquet topological insulators where the TI phase is induced by periodic driving[8]. As to the properties of driven dynamics in the irregular or even chaotic regime which may emerge in quantum systems, this problem with connection to Dirac-Weyl fermions has not been explored, to our knowledge.

For several decades the manifestation of irregular or chaotic regimes of evolution in quantum systems describing the conventional mass particles remains to be an attractive topic for researchers. It is known that the concepts of quantum stochasticity have been successfully introduced and developed for many years.[9, 10, 11] The models of quantum chaos have been also successfully applied on nanoscale for various condensed matter structures [11] including quantum dots.[12] The connections between classical and quantum chaotic systems have been established in such properties like the structure of the quasienergy spectra and the phenomena of quantum diffusion in the Hilbert space. Here the analogies between the diffusion along the resonance eigenstates and along the separatrices in corresponding classical system have been found,[10, 11] including the analogue of Arnol'd diffusion in quantum systems subject to periodic driving.[13]

Much less is known for chaos development in quantum systems without a directly observable classical counterpart, such as systems where the spin degrees of freedom play a significant role and which are described in essentially quantum mechanical way like the systems with spin-orbit coupling (SOC), including the Dirac-Weyl particles with Hamiltonian (1). The importance of such systems in both fundamental and applied fields has been recognized during the last decade, and a significant progress can be observed in corresponding field of nanophysics called spintronics.[14, 15] While the properties of systems with signs of quantum chaos in their spectra are known in detail for numerous nanosize and mesoscopic structures including the quantum dots [12], much less is found about chaos development in quantum system without a directly observable classical counterpart, such as systems with Dirac-Weyl Hamiltonian (1). The presence of SOC in this Hamiltonian leads to correlation between space and spin degrees of freedom and, thus, creates a possibility of non-trivial dynamics or evolution in coupled coordinate and spin channels. It is known that, for example, the combined effects of SOC and the resonance in a multi-level system subject to strong driving may lead to unusual nonlinear behavior in well-known regimes such as quasiclassical dynamics of the electron in a double quantum dot[16], or

the Rabi frequency dependence on the driving strength in the electric dipole spin resonance in a double quantum dot.[17] It was shown also that in double quantum dot with SOC other interesting regimes can develop such as phase synchronization, or even chaotic spin-dependent dynamics.[18] Other examples can be found in a 2D mesoscopic semiconductor quantum dot with SOC,[19] and in the 2D deformed harmonic oscillator potential with SOC[20]. In these studies the non-Poissonian level statistics has been found which indicates the presence of quantum chaos. In our recent paper[21] we have found the development of strongly irregular dynamics in this system under the periodic driving by the electric field, which manifested itself in both charge and spin channels.

The major problem of establishing the quantum-classical correspondence in such spin-dependent systems is the mentioned absence of a direct classical counterpart which create obstacles on describing such systems in terms of the classical chaotic dynamics. The primary tools for overcoming such difficulties are the Floquet analysis for periodic driving [10, 11, 13] and the analysis of transport properties reflecting the regular or chaotic structure of energy spectrum and eigenstates.[12, 22]

In the Floquet analysis one may look on the degree of delocalization of the Floquet eigenstates in the Hilbert space of the basis states or the quasienergy level statistics clearly indicating the possibility of diffusion and chaos development, [10, 11] and on the the direct Fourier analysis of the observables, or quantum mean values.[9, 23] Other tools include the analysis of Poincare sections built in various pairs of coordinates for both coordinate and spin degrees of freedom, not necessarily the canonically conjugated ones, [21, 23] or the tracking of the evolution for the variance for the number of energy levels involved in the dynamics. Here the growth of such variance indicates the development of chaotic regime, and the saturation points on the transition to the quasi-regular mode with finite number of levels participating in the evolution.[13, 21]

In the present paper we address the complex driven dynamics of Dirac-Weyl wavepackets representing the electrons in mesoscopic structures formed at the edge of HgTe/CdTe 2D topological insulator (TI) by magnetic barriers. Such barriers are required due to the effect of Klein tunneling prohibiting the purely electrostatic confinement of the Dirac-Weyl fermions with the Hamiltonian (1). Our general aim is to find out whether the dynamics of a Dirac-Weyl wavepacket with Hamiltonian (1) in a quantum dot (QD) formed at the edge of TI is regular or irregular, if the packet is driven by a monochromatic electric field. To find this, we consider the time evolution of various observables associated with the wavepacket dynamics, their Fourier spectra, and the "phase space" portraits of different pairs of variables, both for coordinate and spin degrees of freedom. We find that certain properties of driven evolution are sustained for wavepackets of different shape and are not smeared by a moderate disorder potential.

This paper is organized as following. In Section 2 we introduce a model of 1D QD at the edge of 2D TI formed in HgTe/CdTe quantum well for the case of magnetic barriers with finite transparency where the electron states have nonvanishing exponentially localized tails inside the barriers. We consider a case of a macroscopic QD with a length $L = 3$ μm in order to obtain a large number of

levels ($N_{\max} \approx 100$) in the TI bulk gap which is desirable to capture the quasi-classical traits of chaos development. Such assumption of a long 1D mesoscopic QD is feasible since the experiments report rather high values of mean free paths in such structures, reaching several microns.[7]. In Section 3 we describe the Floquet eigenstates for the periodically driven single-particle evolution which define the presence of the diffusion in the Hilbert space indicating the possibility of chaotic dynamics. In Section 4 we consider the evolution in the clean limit (no static disorder or noise) for the electron inside the QD, where the electron is represented via the spin polarized wavepacket. We consider the evolution under monochromatic driving electric field, and describe it in terms of phase space plots generalized also for pairs of non-conjugate spin variables, Fourier spectra, diffusion in Hilbert and coordinate space, and Lyapunov exponent. In Section 5 we add the random disorder potential representing the non-ideal character of real nanostructure as well as possible noise in the system and study the driven evolution here. Finally, in Section 6 we present our conclusions.

2. Model

One of the first examples of Dirac-Weyl fermions in condensed matter where the TI-based structures were the HgTe/CdTe 2D quantum wells where the tuning of the well width may create the phase where topologically protected edge states exist.[7, 24] It is known, however, that the applications of TI in nanoelectronic devices require the fabrication of localized small-to-medium size object like quantum dots (QD). Several models of QD formation at the edge of TI where the symmetry protected state exist have been proposed during the last years.[25, 26] Most of them relevant to 1D QD on the edge of 2D TI deal with simplified assumptions of non-transparent magnetic barriers which are required to confine the electrons with massless Dirac-Weyl spectrum.[7] Under such assumptions the spectrum of discrete energy levels inside QD forms a set of equidistant levels located in two ladders above and below the Dirac point of TI where two linear dispersion branches cross.[25] For each level the corresponding eigenstate is a two-component spinor with certain spin polarization, which makes this system a promising candidate for studying there a driven dynamics excited by external electric field tuned to match the interlevel resonance splitting.

In our paper we use the Hamiltonian for the 1D electron in a quantum dot (QD) confining the edge states in 2D HgTe/CdTe topological insulator (TI). It should be mentioned that the form of considered Hamiltonian appear also in other materials with Dirac-Weyls spectra such as graphene where the similar methods of confinement by creating a gap in the spectrum by magnetic field or other mass terms have been offered.[27] Our Hamiltonian is a generalization of the previously derived model for QD with non-transparent barriers[25] for the more realistic case of the barriers with finite transparency reflected in their finite height $M_{0,L}$:

$$H_{QD} = Ak_y\sigma_z - M_0\theta(-y)(\sigma_x \cos \theta_0 + \sigma_y \sin \theta_0) - \quad (2)$$

$$-M_L\theta(y-L)(\sigma_x \cos \theta_L + \sigma_y \sin \theta_L). \quad (3)$$

Here the first term is the effective Dirac-Weyl Hamiltonian (1) for massless edge states propagating on the boundaries of the HgTe/CdTe TI. The parameter A is determined by the HgTe/CdTe quantum well geometry where the two-dimensional electron gas is confined, and for our model we take the value $A = 0.36 \text{ eV} \cdot \text{nm}$ and consider the band gap in HgTe/CdTe to be around 40 meV which corresponds to the quantum well width in the range of 7...8 nm.[7] The second and third term in (3) describe the magnetic barriers located along the TI edge at $y = 0$ and $y = L$ forming a confining QD potential, as it is shown schematically in Fig.1(a). The magnitudes M_0 and M_L of the barriers can be viewed as exchange energies for the interaction between the electron spin and the magnetization inside the barriers. By generalizing previous model,[25] we consider the barriers with finite transparency by choosing finite amplitudes M_0 and M_L which are taken as to cover the whole band gap of the HgTe/CdTe quantum well, and the angles θ_0 and θ_L describe the magnetic domain orientation in the left and right barrier, respectively.

The stationary 1D Schrödinger equation $H_{QD}\Psi = E\Psi$ for the two-component electron spinor $\Psi = (\psi_1(y), \psi_2(y))$ is accompanied by the boundary conditions at $y = 0$ and $y = L$ which can be derived from its integration over infinitesimal small region near the boundary, yielding the requirements

$$\Psi_l(0) = \Psi_r(0), \quad (4)$$

$$\Psi_l(L) = \Psi_r(L) \quad (5)$$

meaning that the wavefunction has to be continuous at the boundaries between the QD and the barriers. The spatial dependence of the solution for a confined state with energy $E < (M_0, M_L)$ inside the barriers at $y < 0$ and $y > L$ has the form of decaying under-the-barrier exponents,

$$\psi_{y<0} = B \left[\begin{array}{c} 1 \\ -\frac{i\sqrt{M_0^2-E^2}+E}{M_0} e^{i\theta_0} \end{array} \right] \exp\left(\frac{\sqrt{M_0^2-E^2}}{A}y\right), \quad (6)$$

$$\psi_{y>L} = D \left[\begin{array}{c} 1 \\ \frac{i\sqrt{M_L^2-E^2}-E}{M_L} e^{i\theta_L} \end{array} \right] \exp\left(-\frac{\sqrt{M_L^2-E^2}}{A}y\right), \quad (7)$$

and the eigenstate inside the QD is the spinor with real wavenumber in its exponents,

$$\psi_{QD} = \left[\begin{array}{c} C_1 e^{iEy/A} \\ C_2 e^{-iEy/A} \end{array} \right], \quad (8)$$

where the coefficients B, C_1, C_2, D are determined from the boundary conditions (5), and the energy E is found from the corresponding secular equation

with Hamiltonian (3). This equation can be solved analytically for the case of non-transparent barriers where the wavefunction does not enter the under-the-barrier region[25, 26] where a sequence of up- and down- strictly equidistant energy levels

$$E_{n_0}^{(0)} = \Delta E^{(0)} \left(n_0 + \frac{1}{2} + \frac{\theta_L - \theta_0}{2\pi} \right), \quad (9)$$

($n_0 = \pm 1, \pm 2, \dots$) is formed with spacing which is independent of $\theta_L - \theta_0$,

$$\Delta E^{(0)} = \frac{\pi A}{L}. \quad (10)$$

In the present paper we will consider the case of parallel orientation $\theta_0 = \theta_L = 0$ since from (9),(10) it follows that different angles of magnetization inside the barriers define mostly the internal structure of corresponding eigenstates and their spin polarization inside the QD, and do not affect the level spacing for the idealized case of non-transparent barriers which defines in our model the primary frequency of driving field. This result is preserved in the case of transparent magnetic barriers considered in our model (3). One may expect that various difference between θ_0 and θ_L will lead to the formation of quantum states with different spatial symmetry, but for our dynamical problem this will produce only quantitative effects on the structure of matrix elements of the external perturbation, and thus only minor effects on the dynamical properties which are in the focus of our studies. Besides, we choose equal amplitudes of magnetic barriers $M_0 = M_L$ which creates a QD with symmetric potential profile, although various combinations of M_0 , M_L , θ_0 , and θ_L can be equally considered if other materials and/or experimental setups are chosen.

In our model the spectrum cannot be found analytically, and has to be obtained from a transcendental equation, which leads in general to a non-equidistant spectrum with non-uniform level spacing ΔE . However, for the mesoscopic QD with $L = 3$ nm where from (10) $\Delta E^{(0)} \approx 0.38$ meV and the condition $\Delta E^{(0)} \ll M_{0,L}$ is satisfied meaning that there are many levels below the barriers are present ($N_{\max} \approx 100$), we have the level spacing ΔE being very close to the equidistant value $\Delta E^{(0)}$ from (10).

The schematic representation of the discrete energy levels inside the QD is shown in Fig.1(b) with a large interlevel distance which is shown as a guide to the eye and not to scale. Together with the discrete levels we show the linear dispersion branches of the Weyl Hamiltonian $H_0 = Ak_y \sigma_z$ describing the edge states[7] before the confining barriers are applied, together with corresponding z -aligned spin mean values S_z and the boundaries of the bulk energy gap $E_g = 40$ meV. This gap allows to limit the barrier width by $M_0 = M_L = E_g/2$ since only the edge states within the bulk gap are relevant for the edge QD where they are not masked by the bulk states.

Our final task considering the model of quantum states inside the QD is the choice of the localized initial condition for the dynamical problem representing an electron which has been injected through one of the magnetic barriers into the dot. We model such condition by a Gaussian spin-polarized wavepacket with two

different widths and center locations with their probability density distribution shown in Fig.1(c) by the solid blue line (1) and dashed red line (2). In terms of the spatial size the packets widths are 1 and 0.1 microns, respectively, which are reasonable values for the semiconductor structures being considered where the mean free path for the electron is about 3 microns.[7] The spin polarization for the corresponding spinor representing the initial packet is chosen as to coincide with the magnetization of the magnetic barrier (or electrode) from which the packet has been injected, that is, the $S_x = 1$ polarization of the left barrier, since the majority of the electrons traveling through the magnetic materials without special tuning usually gain the polarization from the host material. The initial condition $\Psi_0(y)$ needs to be decomposed over the basis states $\Psi_n(y)$ inside the QD for further treatment of its evolution, that is, the coefficients C_n in the decomposition $\Psi_0 = \sum_n C_n \Psi_n(y)$ have to be found by standard methods. The structure of their absolute value distribution $|C_n|^2$ in the space of basis states is shown in Fig.1(d) and (e) for two initial packets from Fig.1(c), respectively. As expected, a wider packet (1) in real space is described by a narrow distribution of $|C_n|^2$ in the Hilbert space compared to the narrow packet (2). We will consider the driven dynamics for both types of wavepackets (1) and (2) in the next sections, and we will see that the difference in their shape in coordinate or Hilbert space leaves certain dynamical features qualitatively the same which allows to consider our finding as relevant for various types of initial conditions.

3. Floquet states

In this and in the following Sections we consider the perturbation for the initial Hamiltonian (3) as a scalar potential $V(y, t)$, in the form of spatially uniform electric field \mathcal{E}_0 created by electrostatic gates. The field is harmonic with frequency $\omega_0 = (E_{n_0+1} - E_{n_0})/\hbar$ matching the level splitting in the region of mostly populated levels by the initial wavepacket, which is the medium part of the spectrum $n_0 \approx 54$ (see Fig.1(d,e)), so

$$V(y, t) = e\mathcal{E}_0 y \cos \omega_0 t, \quad (11)$$

where e is the elementary charge. The periodic driving allows us to apply some of the tools from the Floquet analysis[11, 10, 13, 17, 21] for understanding the system evolution. The part of it which is the most relevant for our system is the structure of the Floquet states where the (s)-th eigenstate is written as a vector $A_n^{(s)}$ in the Hilbert space of the basis states $\Psi_n(y)$. These vectors are the eigenvectors of the one-period propagator matrix $\mathbf{U}(T_0)$ where $T_0 = 2\pi/\omega_0$, which can be constructed from the evolution of the state $\Psi(y, t)$ in the basis of states $\Psi_n(y)$,

$$\Psi(y, t) = \sum_n C_n(t) \Psi_n(y), \quad (12)$$

obeying the non-stationary Schrödinger equation

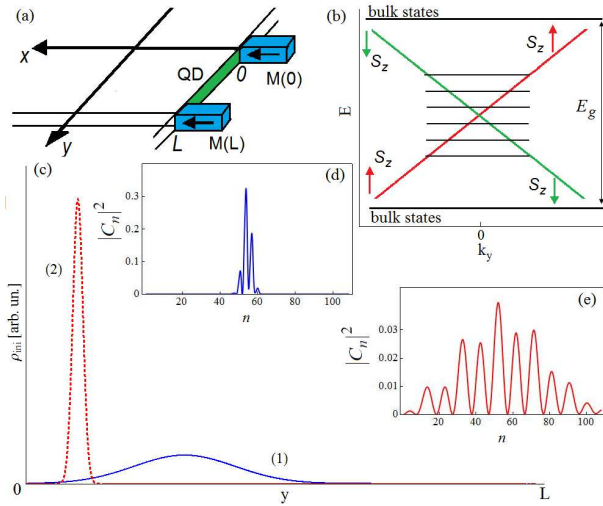


Figure 1: (Color online) (a) Schematic view of a 1D quantum dot (green strip) with length L formed by two magnetic barriers M_0 and M_L at the edge of 2D topological insulator in HgTe/CdTe quantum well. The dot length $L = 3$ μm , the barrier height $M_0 = M_L = E_g/2$ where $E_g = 40$ meV is the band gap for the host material observed for typical HgTe/CdTe quantum well samples, and the arrows inside the barriers represent their polarizations actually considered in our model. (b) Schematic representation of the discrete energy levels inside the QD with the interlevel distance shown as a guide to the eye and not to scale. The linear dispersion branches are shown for the free Weyl Hamiltonian $H_0 = Ak_y\sigma_z$ describing the edge states,[7] with corresponding spin mean values S_z . The boundaries of the bulk energy gap E_g are plotted above and below as horizontal lines. (c) Probability density distribution for Gaussian spin-polarized wavepackets with different widths and center locations representing the initial condition for the dynamics of the electron injected into the QD shown for the wide (solid blue line (1)) and narrow (dashed red line (2)) wavepackets. (d),(e) Distribution of the expansion coefficients $|C_n|^2$ of the initial states from fig. (c) in the space of basis states for (d) the wide initial packet (1) and (e) the narrow initial packet (2), respectively.

$$i\hbar\frac{\partial\Psi}{\partial t} = (H_{\text{QD}} + V(y,t))\Psi, \quad (13)$$

with the initial condition $C_n(0) = \delta_{nn_0}$ considered sequentially for all levels n_0 . [10, 13] The equation (13) is transformed into a system of ordinary linear differential equations for coefficients $C_n(t)$ by projecting it on the basis of the states $\Psi_n(y)$, and this system is solved by standard numerical packages.

The eigenvalues of $\mathbf{U}(T_0)$ labeled by index (s) have the form $\exp(-iE_Q^{(s)}T_0/\hbar)$ where $E_Q^{(s)}$ are the corresponding quasienergies. It is known that the information contained in the quasienergy level spacing distribution can describe the regimes of the driven evolution as regular or chaotic, depending on whether or not such distribution demonstrates the Poissonian or non-Poissonian behavior. [11, 10] In Fig.2(a) we show the level spacing distribution $\rho(\Delta E_Q)$ for three different driving strengths in (11), $\mathcal{E}_0 = 0.2$ V/cm (green dash-dotted curve), $\mathcal{E}_0 = 1$ V/cm (red solid curve), and $\mathcal{E}_0 = 2$ V/cm (blue dotted curve). Although the number of energy levels in our system is quite limited to see a full-developed smooth distribution, it can be seen that for the weak driving the level statistics looks like the Poissonian one with the most of quasienergy levels grouped with small spacing ΔE_Q of the order of 0.005 meV. As the driving increases, the level statistics progressively transforms to a non-Poisson type with the maximum located near 0.03 meV for $\mathcal{E}_0 = 1$ V/cm and near 0.1 meV for $\mathcal{E}_0 = 2$ V/cm. According to the basic concepts of quantum chaos, [11, 10] this result can be viewed as an indication of the transition to chaos in our system with increased amplitude of periodic driving.

Besides the quasienergy spectra, the structure of the Floquet eigenvectors $A_n^{(s)}$ can give a lot of information regarding the possibilities of chaotic regimes for the evolution under periodic driving. [11, 10, 13] In particular, the presence of the states which are extended in the Hilbert space formed by basis functions, that is, described by high values of variance σ_n ,

$$\sigma_n^2 = \sum_n (n - \bar{n})^2 |A_n|^2, \quad (14)$$

where $\bar{n} = \sum_n n |A_n|^2$, corresponds to the regimes of diffusion in the Hilbert space of the initial state along such extended Floquet states, which can be viewed as the quantum counterpart of the classical chaos development. Hence, it is of interest to look at the distribution for all of the quasienergy eigenstates in the (\bar{n}, σ_n) coordinates where \bar{n} is the mean level number measuring the center of the Floquet state in the basis, and σ_n is the variance, or width in the Hilbert space. In Fig.2(b) we plot the (\bar{n}, σ_n) distributions for the Floquet eigenstates for three different driving strengths, $\mathcal{E}_0 = 0.2$ V/cm (green stars), $\mathcal{E}_0 = 1$ V/cm (red filled circles), and $\mathcal{E}_0 = 2$ V/cm (blue open circles). It is clear that the level variance σ_n in general increases with the driving strength which is an expected effect (although a certain saturation with growing \mathcal{E}_0 is present), and the extended states with $\sigma_n \approx 32$ exist at moderate and strong driving, meaning the presence of the diffusion in the Hilbert space into a substantial part of the

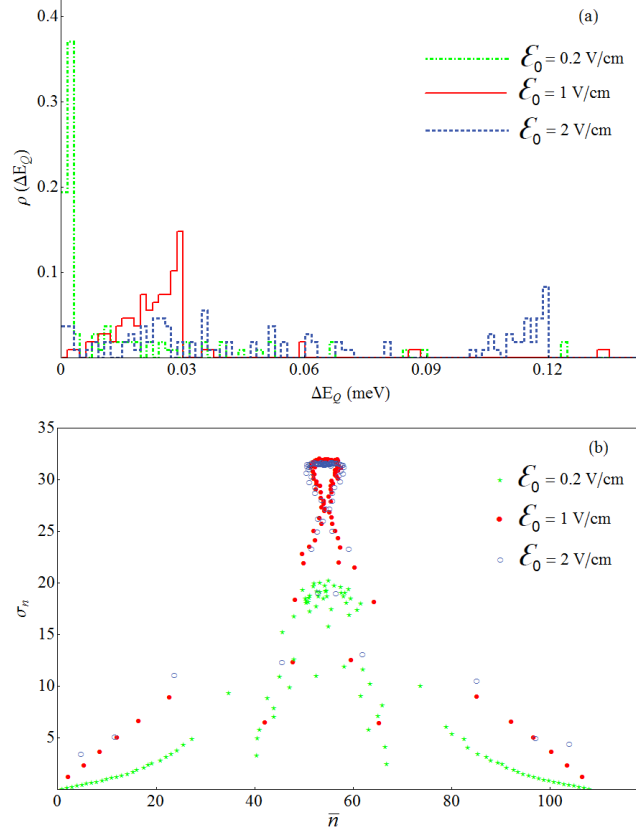


Figure 2: (Color online) (a) Level spacing distribution $\rho(\Delta E_Q)$ for the quasienergy levels for three different driving strengths $\mathcal{E}_0 = 0.2$ V/cm (green dash-dotted curve), $\mathcal{E}_0 = 1$ V/cm (red solid curve), and $\mathcal{E}_0 = 2$ V/cm (blue dotted curve). For the weak driving the level statistics looks like the Poissonian one with the most of quasienergy levels grouped with small spacing ΔE_Q of the order of 0.005 meV. As the driving increases, the level statistics progressively transforms to a non-Poissonian type with maximum shifted to higher values with increased driving, indicating the possible onset of chaotic regime. (b) Distribution of the Floquet quasienergy eigenstates in the (\bar{n}, σ_n) coordinates where \bar{n} is the mean level number measuring the center of the Floquet state in the basis, and σ_n is the variance (width) in the Hilbert space, for driving strengths $\mathcal{E}_0 = 0.2$ V/cm (green stars), $\mathcal{E}_0 = 1$ V/cm (red filled circles), and $\mathcal{E}_0 = 2$ V/cm (blue open circles). The level variance σ_n in general increases with the driving strength, and the extended states with $\sigma_n \approx 32$ exist at moderate and strong driving, meaning the presence of the diffusion in the Hilbert space into a substantial part of the spectrum and reflecting the possibility of irregular, or chaotic dynamics.

spectrum totaling 108 levels for the present set of model parameters. We may see from Fig.2(b) that the difference between the quasienergy state statistics for $\mathcal{E}_0 = 1$ V/cm and $\mathcal{E}_0 = 2$ V/cm is only quantitative, so only moderate driving fields not exceeding the scale of 1 V/cm are required for the excitation of the most interesting regimes in our system, which is desirable for the possible device applications. We thus can conclude that the analysis of the Floquet eigenstates demonstrates the possibility of excitation of the Hilbert space diffusion regimes for driven dynamics if the initial states are located in the region of maximum variance σ_n near the center of the spectrum. In the next Section we will confirm this assumption by direct integration of the nonstationary Schrödinger equation with Hamiltonian $H_{qd} + V(y, t)$. The reason for such approach is that a substantial part of the evolution takes place between the stroboscopic moments of time $T_n = nT_0$ which are in the focus of the Floquet stroboscopic approach. To obtain more detailed picture, we proceed with direct numerical integration for continuous time with suitable time grid catching all of the essential non-vanishing higher harmonics of ω_0 , and having also a perfect match between the continuous and Floquet approaches.

4. Evolution in the clean limit

We begin with the analysis of the driven evolution of the wide wavepacket (see Fig.1(c),(d)) which is described by the Schrödinger equation (13) with moderate driving amplitude $\mathcal{E}_0 = 1$ V/cm of the driving electric field (11). The initial state $C_n(0)$ occupies a narrow part of the Hilbert space near the center of the spectrum, as it can be seen in Fig.1(d). We solve the equations of motion for $C_n(t)$ from several hundreds to several thousands of periods $T_0 = 2\pi/\omega_0$ which is the unit of time in our model, where $\hbar\omega_0$ is the spacing between a selected pair of levels near the center of the spectrum.

The evolution parameters in which we are interested include the quantum mechanical mean values (observables) both for coordinate and spin degrees of freedom, and their Fourier power spectra

$$I_\xi(\omega) = \left| \int_{-\infty}^{+\infty} \xi(t) e^{-i\omega t} dt \right|^2, \quad (15)$$

where ξ is the variable of interest. Since we have obviously considered large, but finite intervals of time, the Fourier power spectra (15) were calculated by the Fast Fourier Transform with limits of time actually used in our simulations of dynamics. As to the analogue of the classical phase space dynamics, the spin-dependent system with Hamiltonian (3) provides us with an interesting example of the "conjugate" pair of observables, the coordinate one is the usual space coordinate, y , while the "velocity"

$$v_y = \frac{1}{\hbar} \frac{\partial H_{qd}}{\partial k_y} = v_F \sigma_z, \quad (16)$$

where $v_F = A/\hbar = 5.3 \cdot 10^7$ cm/s is the Fermi velocity. This result means that the momentum is effectively represented on the "phase space plot" by the z component of spin, so the first pair of the variables considered by us is (y, S_z) . The second pair of variables to be plotted together is the in-plane spin projection represented by the (S_x, S_y) spin components. This pair of variables has been considered in several studies on the spin-resolved systems,[16, 21, 23] and is convenient in representing, for example, the in-plane spin precession. The initial state of the wavepacket injected from the left barrier into the QD is characterized by the spin polarization in units of $\hbar/2$ as $S_x = 1, S_y = S_z = 0$. We have found that for all the basis states (8) the mean spin is always in the plane of the 2D TI, that is, $S_z = 0$. However, if a time-dependent mixture (12) of such states is considered formed by the initial packet or by the non-stationary driving $V(y, t)$, the resulting spinor wavefunction may correspond to the state where the out-of-plane S_z spin component is present. We will discuss it in detail below.

The evolution of the variance of the level number $\sigma_n(t)$ (see Eq.(14) where $A_n \rightarrow C_n(t)$) describes the spreading of the initial state $C_n(0)$ in the Hilbert space of the basis states. Also, we are interested in the dynamics of the variance σ_y for packet width in the coordinate space,

$$\sigma_y^2(t) = \langle (y - \langle y(t) \rangle)^2 \rangle, \quad (17)$$

where $\langle \dots \rangle$ stands for standard quantum mechanical averaging with the wavefunction $\Psi(y, t)$. It is also of interest to look at the spatial distributions along the QD for the charge density $\rho(y, t_0)$ and some of the spin density components $S_i(y, t_0)$, $i = x, y, z$, at certain moments of time. The spatial profiles of charge and spin density help in understanding on which spatial scale one can measure the charge and spin spots in actual experimental setups.

We consider the time interval of 400 periods of driving field with 200 points per period for the graphical representation. These parameters cover both the time span needful for the stationary regime of the dynamics to be established, and the time grid which catches the significant non-vanishing Fourier components of the evolution of observables.

In Fig.3 we show the results for the driven evolution for the initial state represented by the wide wavepacket from Fig.1(c). The initial point at $t = 0$ is marked as the black circle "A". (a) the "phase space" plot of evolution in the (y, S_z) coordinates and (b) the in-plane spin precession in the (S_x, S_y) plane demonstrate a complex and irregular character of the driven evolution. In particular, the regular trajectories in Fig.3(a) are accompanied by the surrounding areas of the "chaotic sea", although the general oscillating character of the wavepacket evolution is still visible. The onset of irregular motion is further pronounced in the in-plane spin dynamics shown in Fig.3(b). The spin evolution becomes largely irregular. A large clustering area near the origin of spin axes indicates a tendency of reduction of the in-plane spin maximum values during the driven evolution which can be viewed as a manifestation of the spin relaxation phenomena.[14, 15] As to the absence of such relaxation

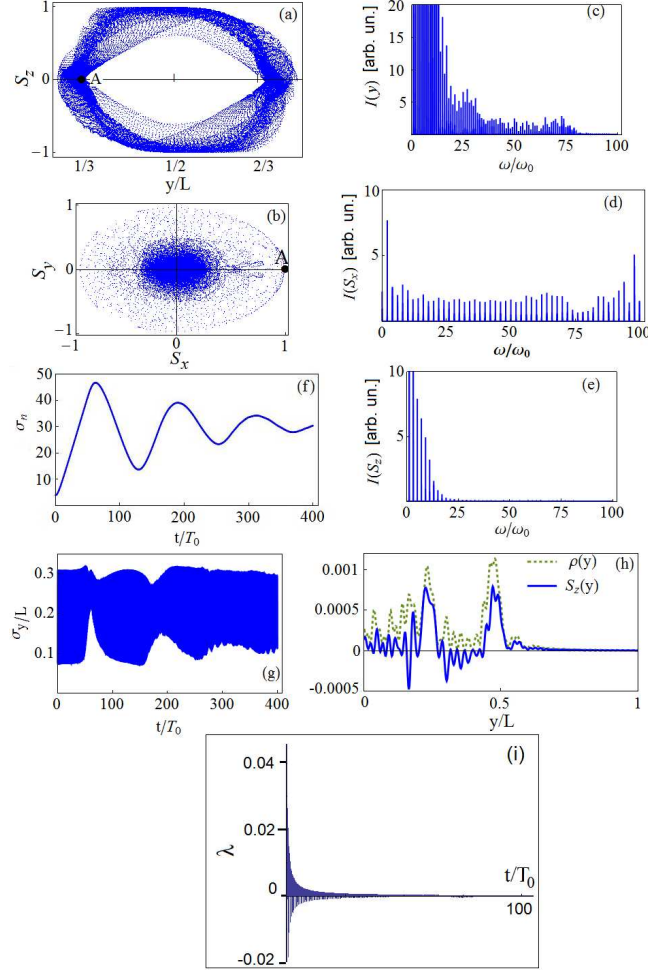


Figure 3: (Color online) (a) Evolution in the "phase space" of the (y, S_z) variables representing classical coordinate and momentum for the amplitude $\mathcal{E}_0 = 1$ V/cm of the driving electric field (11), (b) Evolution of the in-plane spin components (S_x, S_y) . The initial point at $t = 0$ is shown as black circle marked by "A". The evolution of both coordinate and spin shows the coexistence of both regular and chaotic regimes seen in the presence of both regular trajectories and the large areas of "stochastic sea", especially for the spin variables. The in-plane spin components demonstrate the tendency of clustering near the zero values with growing time, which is the manifestation of the in-plane spin relaxation. (c)-(e) Fourier power spectra (15) for the coordinate y and two spin components S_x and S_z . Large number of harmonics of the driving frequency indicates the onset of strongly irregular motion. (f) The evolution in the Hilbert space plotted as a number of levels effectively participating in the dynamics shows the linear growth at the beginning of the evolution which corresponds to the chaotic regime. Later the level number saturates near a stable value corresponding to the width of the Floquet states in Fig.2. (g) The packet half-width variance describing the spreading of the wavepacket in the real space inside the QD. The initial half-width (see Fig.1(c), packet (1)) does not grow with time, and, as for the free evolution, at certain moments of time the packet is narrowed. (h) Charge density $\rho(y)$ (green dashed curve) and the $S_z(y)$ component of spin density (blue solid curve) inside the QD taken at specific moment of time $t = 395T_0$. The packet is spreaded along the QD, but the major part of the charge and spin density are concentrated on the width comparable with the width of the initial packet. (i) Evolution of the Lyapunov exponent (18) for two initially close wavepackets. At the beginning of the evolution this exponent takes also positive values indicating the presence of chaotic regime, and later it decreases to zero when the quasi-regular quantum dynamics is established.

for the out-of-plane S_z component, it can be attributed to the special form of the initial Hamiltonian (3) where S_z plays a role of the electron velocity and thus is non-vanishing in the absence of the momentum or energy relaxation mechanisms.

The manifestation of chaotic or at least strongly irregular regimes for the driven evolution is supported by the Fourier power spectra for the coordinate and spin observables plotted in Fig.3(c)-(e). One may see that the driving induces a large number of harmonics of driving frequency ω_0 both for coordinate and spin, especially the in-plane component S_x (and similarly for S_y which is not shown here). Although the dynamics is dominated by the nearly equidistant character of energy levels leading to the nearly equidistant sequence of harmonics of ω_0 in the power spectra, and thus the Fourier harmonics do not fill frequency bands continuously, the presence of large number of harmonics is a strong indication of irregular dynamics.[9, 16, 21]

The concept of irregular dynamics or chaos development can be supported by analysis of the driven evolution in the Hilbert space of basis states where the onset of chaos usually corresponds to the growth in time of the number of energy levels involved into evolution, which is sometimes called as manifestation of quantum Arnol'd diffusion.[13] Our Floquet analysis of the quasienergy eigenfunctions described in Sec.III indicates that the periodic driving with amplitudes of 1...2 V/cm may induce the formation of the Floquet states which are deeply extended into a substantial part of the energy spectrum, see Fig.2. Thus, we may expect the number of level variance σ_n measuring the number of levels involved into evolution to be as high as the maximum number reached by the Floquet states. This assumption is confirmed by the plot of $\sigma_n(t)$ in Fig.3(f) where almost linear growth of level number is present at the initial stage of evolution where the quantum-classical correspondence is mostly pronounced.[9, 11, 10] Such growth is usually attributed to the onset of chaotic dynamics, or diffusion in Hilbert space. After some time, however, the discrete character of the quantum mechanical spectrum of a finite motion inside QD leads to the saturation of the level number involved in the evolution, and the diffusion in the Hilbert space effectively stops.[13] This can be seen in Fig.3(f) where the linear growth of σ_n transforms into oscillations with stable mean value. We can say that the chaotic behavior in our quantum system has a transient nature.

As to the dynamics in the real space inside the QD, the evolution of the packet half-width is presented in Fig.3(g). The packet width essentially does not grow with time both for the free and driven case, and the packet at each moment of time occupies effectively only a limited area inside the QD. This finding is illustrated by an example of the spin and charge density distributions inside the QD shown for $t = 395T_0$ in Fig.3(h) as blue solid and green dashed lines, respectively. One may see that the packet occupies a substantial part of the QD, however, its effective width has the value close to the width of the initial packet, see Fig.1(c), wavepacket (1). As we have mentioned earlier, such stable behavior of the packet width during the driven evolution can be attributed to the nearly equidistant character of the energy levels of the system which can trigger certain properties of the coherent states in the driven evolution.

Another possible manifestation of chaos is the presence of positive Lyapunov exponents[9, 10] which measure the rate of divergence of two initially close trajectories in the phase space,

$$\lambda = \lim_{t \rightarrow \infty} \frac{1}{t} \log \frac{d(t)}{d(0)}, \quad (18)$$

where $d(t)$ and $d(0)$ are the present and initial distances, respectively. The infinite limit in (18) can be tracked also by a continuously monitoring with growing time where $\lambda = \lambda(t)$ tracks local transition between regular and chaotic regimes. In Fig.3(i) we plot the dependence of $\lambda(t)$ for two initially close wavepackets which mean values of coordinate are shifted slightly along y at $t = 0$. One can see that at the beginning of the evolution the region with positive $\lambda(t)$ indeed exists which corresponds to the linear growth of the level number σ_n involved into the dynamics, see Fig.3(f). Both these plots support the presence of chaotic dynamics at the initial stage of the evolution when the discrete character of the quantum spectrum has not yet manifested itself so much. After the initial transient period the evolution tends to transform to a quasi-regular regime with the stable number of levels involved into dynamics, and the Lyapunov exponent reduces to zero, as in can be seen in Fig.3(i). It should be noted that such behavior is known in quantum systems with irregular dynamics.[9, 11, 10, 13] However, the results obtained there were mainly for the spinless systems with quadratic spectrum having a certain classical analogue. It is of big importance both for fundamental quantum physics and its applications in spintronics and nanoelectronics to understand such properties in essentially quantum spin-dependent systems, including the massless Hamiltonians for particles inside topological insulators.

5. Evolution in the presence of a disorder

In this Sec we insert an additional stationary disorder potential

$$U_d(y) = U_0 f(y) \quad (19)$$

into the r.h.s. of the non-stationary Schrödinger equation (13) where the potential amplitude U_0 is multiplied by a random function $f(y)$ described by a uniform random distribution from 0 to 1 along the QD where $0 \leq y \leq L$. The matrix elements of $U_d(y)$ contribute to the dynamics of the coefficients $C_n(t)$ for the wavefunction (12) together with the ones from the driving term $V(y, t)$. We consider an example of the amplitude $U_0 = 0.5$ meV which is comparable with typical interlevel distance (10) equal to 0.38 meV, i.e. we insert a moderate disorder. This can be justified by a typical high quality and high mobility of samples usually fabricated and studied in the experiments with TI,[7] which have the mean free path of the order of the QD length L , and low temperatures of around or below 1 K which produces the level broadening of the order of 0.05 meV. For the initial condition we put a narrow wavepacket, see the packet

profile shown by curve (2) in Fig.1(c). We take the same driving amplitude $\mathcal{E}_0 = 1$ V/cm, and the same other parameters as in the previous Sec.

One can expect certain modifications of the evolution for both coordinate and spin degrees of freedom, when the disorder amplitude U_0 exceeds the energy of the driving field. In Fig.4 we show the evolution of the narrow wavepacket under the driving with $\mathcal{E}_0 = 1$ V/cm, with a disorder amplitude $U_0 = 0.5$ meV which exceeds the typical energy of the driving field $e\mathcal{E}_0L = 0.3$ meV. One can see that the disorder leads to more irregular phase portraits for the evolution in the (y, S_z) and (S_x, S_y) coordinates shown in Fig.4(a),(b). In particular, the in-plane spin components (S_x, S_y) demonstrate a more pronounced tendency to cluster near the coordinate origin $(0, 0)$ with growing time meaning that the effective in-plane spin relaxation is enhanced by the presence of a disorder. As to the off-plane spin component S_z , it still demonstrates a full-scale oscillating behavior representing the electron velocity in our model, but within a well-established chaotic sea visible in the (y, S_z) plot. This dynamics is supported by the Fourier power spectra shown in Fig.4(c)-(e) where the spin components demonstrate a more quickly vanishing spectra due to the spin relaxation compared to the coordinate one. The disorder leads to an interesting effect on the number of levels σ_n effectively involved in the evolution which is shown in Fig.4(f). Starting from the initially high number of basis states present in the decomposition of a narrow wavepacket, this number begins to decrease progressively, with the average level number (not shown) moving down from the Dirac point. Such a form of localization in the Hilbert space can be viewed as an example of dynamical localization observed in quantum systems with chaotic behavior.[11, 10] Finally, the variance of the packet half-width shown in Fig.4(g) shows the oscillating behavior with saturating amplitude which again demonstrates the effect of the wavepacket maximum width stability induced by the periodic driving, which is maintained even in the presence of a strong disorder. An example of the charge $\rho(y)$ and spin density $S_z(y)$ distributions at the end of the observation frame $t = 395T_0$ shown in Fig.4(h) supports this finding, demonstrating a well-localized packet near the edge of the QD.

We believe that the properties of the wavepacket evolution observed in our model which include the mutual effects of periodic driving and disorder on charge and spin evolution as well on the regular and irregular character of the dynamics can be of interest for further applications of our finding in the development of both fundamental aspects of quantum evolution and for the applications.

6. Conclusions

We have studied the dynamics of Dirac-Weyl wavepackets driven by periodic electric field in a mesoscopic quantum dot formed at the edge of two-dimensional HgTe/CdTe topological insulator, where the motion of carriers is less sensitive to disorder and impurity potentials. It was found that the interplay of strongly coupled spin and charge degrees of freedom creates the regimes of both regular and transiently irregular dynamics with certain universal properties manifested both in the clean limit and in the presence of the disorder. The effects of

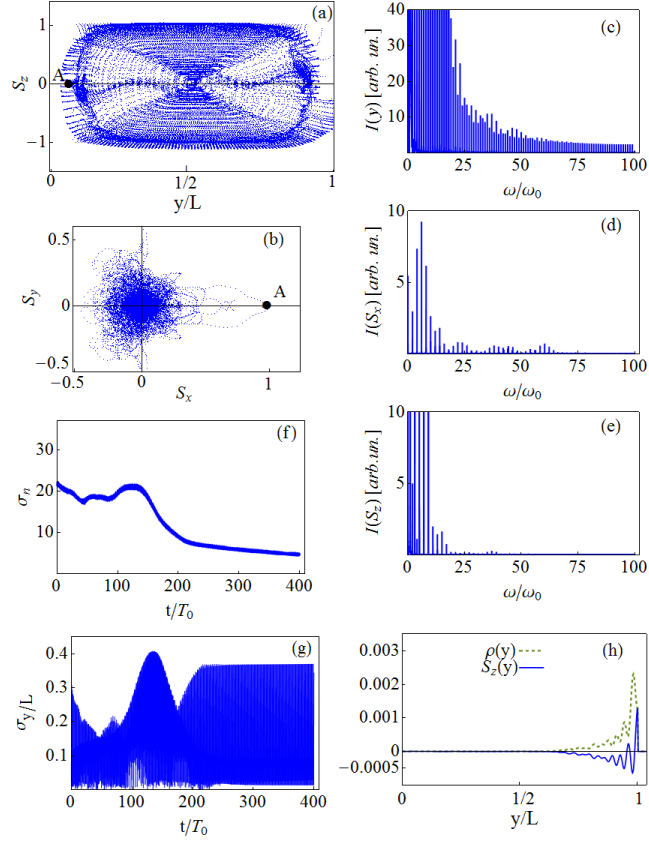


Figure 4: (Color online) Same as in Fig.3 but for a narrow wavepacket (see Fig.1(c),(e)) taken as initial condition, and in the presence of the disorder potential (19) with amplitude $U_0 = 0.5$ meV. (a),(b) Coordinate and spin observables shown in the form of phase portraits. The in-plane spin components show an enhanced tendency of clustering near the zero values with growing time, which is the manifestation of the in-plane spin relaxation. (c)-(e) Fourier power spectra showing the behavior where the disorder can overcome the driving and enhance the in-plane spin relaxation. (f) Evolution in the Hilbert space of σ_n demonstrates the decreasing number of basis states participating in the evolution which can be viewed as an example of dynamical localization. (g) The packet half-width dynamics shows the amplitude stability on long times (h) An example of charge and spin density for $t = 395T_0$ demonstrates a well-localized packet even at the presence of strong disorder potential.

random disorder potential are found to enhance the in-plane spin relaxation. The dynamical properties of regular and chaotic behavior of charge and spin in these structures may be of interest for future progress in both quantum dynamics on the nanoscale and in the applied nanoscience such as spintronics and nanoelectronics.

Acknowledgements

The authors are grateful to V.Ya. Demikhovskii, A.I. Malyshev, A.M. Shtanin, E.Ya. Sherman, M.V. Ivanchenko, and S. Denisov for stimulating discussions. The work is supported by the RFBR Grants No. 13-02-00717a, 13-02-00784a, 14-02-31637-mol-a, by the University of Nizhny Novgorod and the RAS Joint Laboratories Project, and by the "Dynasty" Foundation.

References

References

- [1] G.E. Volovik, *The Universe in a Helium Droplet*, Clarendon Press, Oxford, 2003.
- [2] P.B. Pal, *Am. J. Phys.* 79 (2011) 485.
- [3] G.E. Volovik, M.A. Zubkov, *JETP Letters* 99 (2014) 481.
- [4] Y. Cheng, O.C.W. Kong, *Ann. Phys.* 348 (2014) 315.
- [5] Y. Chen, D.L. Bergman, and A.A. Burkov, *Phys. Rev. B* 88 (2013), 125110.
- [6] I. Romanosvky, C. Yannouleas, and U. Landman, *Phys. Rev. B* 87 (2013), 165431.
- [7] B.A. Bernevig, *Topological Insulators and Topological Superconductors*, Princeton University Press, Princeton, 2013; S.Q. Shen, *Topological insulators. Dirac equation in Condensed Matter*, Springer Series in Solid-State Science, Springer-Verlag Berlin Heidelberg, 2012; M.Z. Hasan and C.L. Kane, *Rev. Mod. Phys* 82 (2010) 3045; X-L Qi and S-C Zhang, *Rev. Mod. Phys.* 83 (2011) 1057.
- [8] N.H. Lindner, G. Refael, V. Galitski, *Nat. Phys.* 7 (2011) 490.
- [9] M.C. Gutzwiller, *Chaos in Classical and Quantum Mechanics*, Springer-Verlag, New York, 1990.
- [10] L.E. Reichl, *The Transition to Chaos. Conservative Classical Systems and Quantum Manifestations*, 2nd Ed., Springer-Verlag, New York, 2004.
- [11] H-J. Stöckmann, *Quantum Chaos: An Introduction*, Cambridge University Press, 1999.

- [12] K. Nakamura and T. Harayama, *Quantum Chaos and Quantum Dots*, Oxford University Press, New York, 2004.
- [13] V.Ya. Demikhovskii, F.M. Izrailev, and A.I. Malyshev, *Phys. Rev. Lett.* 88 (2002) 154101; *Phys. Rev. E* 66 (2002) 036211; A.I. Malyshev and L.A. Chizhova, *J. Exp. Theor. Phys.* 110 (2010) 837.
- [14] I. Zütić, J. Fabian, and S. Das Sarma, *Rev. Mod. Phys.* 76 (2004) 323.
- [15] *Spin physics in semiconductors*, ed. by M.I. Dyakonov, Springer-Verlag Berlin Heidelberg, 2008.
- [16] D. V. Khomitsky and E. Ya. Sherman, *Phys. Rev. B* 79 (2009) 245321.
- [17] D.V. Khomitsky, L.V. Gulyaev, and E.Ya. Sherman, *Phys. Rev. B* 85 (2012) 125312.
- [18] L. Chotorlishvili, Z. Toklikishvili, A. Komnik, and J. Berakdar, *Phys. Lett. A* 377 (2012 69); *J. Phys.: Condens. Matter* 24 (2012) 255302.
- [19] K.-F. Berggren and T. Ouchterlony, *Found. Phys.* 31 (2001) 233.
- [20] O.V. Marchukov, A.G. Volosniev, D.F. Fedorov, A.S. Jensen, and N.T. Zinner, *J. Phys. B: At. Mol. Opt. Phys.* 47 (2014) 195303.
- [21] D.V. Khomitsky, A.I. Malyshev, E.Ya. Sherman, and M. Di Ventura, *Phys. Rev. B* 88 (2013) 195407.
- [22] K.-F. Berggren, A.F. Sadreev, and A.A. Starikov, *Phys. Rev. E* 66 (2002) 016218; E.N. Bulgakov, D.N. Maksimov, and A.F. Sadreev, *Phys. Rev. E* 71 (2005) 046205; E.N. Bulgakov and I. Rotter, *Phys. Rev. E* 73 (2006) 066222; K.-F. Berggren, D.N. Maksimov, A.F. Sadreev, R. Höhmann, U. Kuhl, and H.-J. Stöckmann, *Phys. Rev. E* 77 (2008) 066209.
- [23] Z. Yang, S. Zhang, and Y. C. Li, *Phys. Rev. Lett.* 99 (2007) 134101.
- [24] B.A. Bernevig, T.L. Hughes, and S.-C. Zhang, *Science* 314 (2006) 1757; M. König, H. Buhmann, L.W. Molenkamp, T.L. Hughes, C.-X. Liu, X.-L. Qi, and S.-C. Zhang, *J. Phys. Soc. Jpn* 77 (2008) 031007.
- [25] C. Timm, *Phys. Rev. B* 86 (2012) 155456.
- [26] A. Kundu, A. Zazunov, A.L. Yeyati, T. Martin, and R. Egger, *Phys. Rev. B* 83 (2011) 125429; G. Dolcetto, N. Traverso Ziani, M. Biggio, F. Cavaliere, and M. Sasseti, *Phys. Rev. B* 87 (2013) 235423; G.J. Ferreira and D. Loss, *Phys. Rev. Lett.* 111 (2013) 106802; C. Ertler, M. Raith, and J. Fabian, *Phys. Rev. B* 89 (2014) 075432.
- [27] G. Giavaras, P.A. Maksym, and M. Roy, *J. Phys. Cond. Mat.* 21 (2009) 102201; G. Giavaras and F. Nori, *Phys. Rev. B* 83 (2011) 165427; G. Giavaras and F. Nori, *Phys. Rev. B* 85 (2012) 165446.